INTERNATIONAL JOURNAL FOR NUMERICAL METHODS IN ENGINEERING
Int. J. Numer. Meth. Engng 2007; **70**:913–933
Published online 2 November 2006 in Wiley InterScience (www.interscience.wiley.com). DOI: 10.1002/nme.1895

A bridging domain and strain computation method for coupled atomistic–continuum modelling of solids

Sulin Zhang[1,2], Roopam Khare[1], Qiang Lu[1] and Ted Belytschko[1,*,†]

[1]*Department of Mechanical Engineering, 2145 N. Sheridan Rd., Northwestern University, Evanston, IL 60208-3111, U.S.A.*
[2]*Department of Mechanical Engineering, 204 Mechanical Engineering Building, University of Arkansas, Fayetteville, AR 72701, U.S.A.*

SUMMARY

We present a multiscale method that couples atomistic models with continuum mechanics. The method is based on an overlapping domain-decomposition scheme. Constraints are imposed by a Lagrange multiplier method to enforce displacement compatibility in the overlapping subdomain in which atomistic and continuum representations overlap. An efficient version of the method is developed for cases where the continuum can be modelled as a linear elastic material. An iterative scheme is utilized to optimize the coupled configuration. Conditions for the regularity of the constrained matrices are determined. A method for computing strain in atomistic models and handshake domains is formulated based on a moving least-square approximation which includes both extensional and angle-bending terms. It is shown that this method exactly computes the linear strain field. Applications to the fracture of defected single-layer atomic sheets and nanotubes are given. Copyright © 2006 John Wiley & Sons, Ltd.

Received 10 August 2006; Accepted 30 August 2006

KEY WORDS: bridging domain; graphene sheets; moving least square; molecular mechanics

1. INTRODUCTION

Modelling of material failure often involves phenomena simultaneously occurring at multiple length scales. On the one hand, such behaviour cannot be described by continuum mechanics without

*Correspondence to: Ted Belytschko, Department of Mechanical Engineering, 2145 N. Sheridan Rd., Northwestern University, Evanston, IL 60208-3111, U.S.A.
†E-mail: tedbelytschko@northwestern.edu

Contract/grant sponsor: NASA University Research, Engineering and Technology Institute on Bio Inspired Materials (BIMat); contract/grant number: NCC-1-02037

resorting to phenomenological descriptions since fracture is intrinsically a bond breaking phenomenon. On the other hand, computational costs limit atomistic simulations to small subdomains relative to realistic specimens, even for specimens such as nanotubes and nanorods. It is thus desirable to develop multiscale material modelling approaches coupling continuum and atomistic models.

Extensive work has been done in the development of multiscale modelling approaches for linking atomistic with macroscopic models. Among them are the coupled length scale method [1, 2], the bridging method [3, 4], the bridging domain method [5, 6], the method coupling atomistic and discrete dislocation plasticity [7], and the homogenization [8]. Despite different treatments in the coupling strategy, these methods share basic principles, and typically have three components: a finite element representation for continuum subdomains where the deformation field is smooth and homogeneous; a molecular mechanics/dynamics description for atomistic subdomains in which bond breaking is expected; a strategy to couple these two representations. Differences in the available coupling methods are the specifics of the coupling strategies, which have been extensively reviewed elsewhere [9–11].

We here present extensions of the bridging domain method of Belytschko and Xiao [5] and an analysis of some of its properties. Dhia and Rateau [12] originated this method for the purpose of joining finite-element meshes and called it the Arlequin method. These methods are essentially overlapping domain decomposition methods; they are called 'handshake' methods in [2], although no constraints were specified in the handshake domain. So it is unclear how continuity was enforced between subdomains. For many nanoscale fracture problems, a large portion of the computational domain undergoes homogeneous deformation, and bond forming/breaking takes place only within a small subdomain. The primary function of the continuum domain is to provide the appropriate boundary conditions for the atomistic subdomain and to suppress the surface effects. The aim of the proposed multiscale method is to solve coupled molecular mechanics/continuum mechanics efficiently. This method offers atomistic resolution of deformation in subdomains encompassing defects such as vacancies, interstitials, dislocations, and crack tips, and treats the remainder of the domain with crystal elasticity. Displacement compatibility conditions are imposed in the overlapping subdomain by the Lagrange multiplier method. The resulting governing equations are coupled through the internal forces corresponding to Lagrange multipliers. The governing equations can further be simplified provided that the continuum subdomain is linear elastic. This method matches the corresponding results of a fully atomistic model with reasonable accuracy, and greatly reduces the computational costs.

An attractive feature of the method is that it does not require the finite element mesh to match the lattice spacing of the atomic model. Thus, it is easy to link various atomistic models, even models of amorphous solids, with finite element models. Furthermore, the approach allows finite element models to be replaced by atomistic models wherever it is needed by zeroing the material properties of the target subdomain of finite element mesh and overlaying the atomistic model on the desired subdomain.

In addition, a method is presented for obtaining continuous strain fields for atomistic models. The so-called 'atomistic strains' have previously been developed by Mott *et al.* [13], but they were based on Voronoi tessellations and were only defined at atomic positions. Here, we employ a moving least-square (MLS) approximation to compute the atomistic strains. It is shown that for an atomistic displacement corresponding to a linear field, the exact strain field is computed by this method.

DOI: 10.1002/nme

2. METHOD

The coupled method consists of three components: the atomistic model; the continuum model; and the coupling strategy. Both the atomistic and continuum framework we adopt here are taken from the literature. Therefore, we will focus on the coupling of the two models, which is described in the following subsections. For clarity, we use Greek indices (α, β, γ) to denote atoms, capital indices (I, J, K) to denote the finite element nodes, and lower-case indices (i, j, k) to denote the components of vectors and tensors.

2.1. Coupling

Consider a solid body subjected to prescribed traction $\bar{\mathbf{t}}^0$ on the undeformed surface Γ_0^{t}, and prescribed displacement $\bar{\mathbf{u}}$ on Γ_0^{u}. The entire domain is decomposed into three subdomains: an atomistic subdomain Ω_0^{A}; a continuum subdomain, Ω_0^{C}, and the overlapping subdomain, $\Omega_0^{\mathrm{H}} = \Omega_0^{\mathrm{A}} \cap \Omega_0^{\mathrm{C}}$, where the atomistic and continuum models overlap, i.e. the handshake domain. The superscripts 'C' (continuum) and 'A' (atomistic) identify the associated variables. We assume that Γ_0^{t} is restricted to the boundary of the continuum subdomain and the atomistic subdomain is traction free. Under external loading, each material point $\mathbf{X} \in \Omega_0^{\mathrm{C}}$ in the initial, undeformed configuration moves to its current position $\mathbf{x}$ according to a deformation map: $\mathbf{x} = \boldsymbol{\phi}(\mathbf{X}, t)$. The initial position of atom α is denoted by $\mathbf{X}_\alpha$, and its current position is denoted by $\mathbf{x}_\alpha$. The total free energy (E_{total}) is sum of the strain energy of the continuum subdomain (E_{CM}), and the potential energy of atomistic subdomain (E_{MM}), minus the external work (E_{ext}) on both subdomains:

$$E_{\mathrm{total}} = E_{\mathrm{MM}} + E_{\mathrm{CM}} - E_{\mathrm{ext}} \tag{1}$$

where

$$E_{\mathrm{MM}} = \sum_{\alpha \in \Omega_0^{\mathrm{A}}} \left[\sum_{\beta > \alpha} w^{\mathrm{A}} \left(\frac{1}{2}(\mathbf{X}_\alpha + \mathbf{X}_\beta) \right) V_{\alpha\beta} \right] \tag{2}$$

$$E_{\mathrm{CM}} = \int_{\Omega_0^{\mathrm{C}}} w^{\mathrm{C}}(\mathbf{X}) W(\mathbf{F}(\boldsymbol{\phi}(\mathbf{X}))) \, \mathrm{d}\Omega_0 \tag{3}$$

and

$$E_{\mathrm{ext}} = \int_{\partial\Omega_{\mathrm{t}}^{\mathrm{C}}} w^{\mathrm{C}}(\mathbf{X}) \bar{\mathbf{t}}^0 \cdot \mathbf{u} \, \mathrm{d}\Gamma_0 \tag{4}$$

In the above expressions, $V_{\alpha\beta}$ is the atomistic interaction potential between atoms α and β, W is the strain-energy density function, $\partial\Omega_{\mathrm{t}}^{\mathrm{C}}$ is the portion of the boundary of Ω_0^{C} where the traction $\bar{\mathbf{t}}^0$ is applied, $\mathbf{u} = \boldsymbol{\phi} - \mathbf{X}$ is the displacement vector, and $\mathbf{F}$ is the deformation tensor given by

$$\mathbf{F} = \frac{\partial \boldsymbol{\phi}}{\partial \mathbf{X}} = \mathbf{I} + \frac{\partial \mathbf{u}}{\partial \mathbf{X}} \tag{5}$$

and $\mathbf{I}$ is the identity tensor. It should be noted that, in order to avoid double counting of the atomistic and the continuum energies in the handshake domain, these energy terms are weighted

DOI: 10.1002/nme

based on the positions at which these values are evaluated. The weight functions, w^{C} and w^{A}, vary linearly across the handshake domain

$$w^{\mathrm{C}}(\mathbf{X}) = 1 - w^{\mathrm{A}}(\mathbf{X}) = \begin{cases} 1 & \mathbf{X} \in \Omega_0^{\mathrm{C}} \backslash \Omega_0^{\mathrm{H}} \\ \|\mathbf{X} - \mathbf{X}_{\mathrm{B}}\|/L & \mathbf{X} \in \Omega_0^{\mathrm{H}} \\ 0 & \mathbf{X} \in \Omega_0^{\mathrm{A}} \backslash \Omega_0^{\mathrm{H}} \end{cases} \tag{6}$$

We assume that the atomistic domain is convex and sufficiently regular so that the parameter w^{C} can be uniquely determined by the nearest point projection of $\mathbf{X}$ onto the boundary of Ω_0^{C}, denoted by $\mathbf{X}_{\mathrm{B}}$. The variable L is the distance between the inner and outer boundaries of the handshake domain along the vector $\mathbf{X} - \mathbf{X}_{\mathrm{B}}$. The boundary $\partial\Omega_{\mathrm{t}}^{\mathrm{C}}$ that is overlapped by the atomistic model is a traction-free boundary ($\bar{\mathbf{t}} = 0$).

Coupling of the atomistic and continuum models is achieved by approximately enforcing displacement compatibility in the handshake domain:

$$\boldsymbol{\phi}(\mathbf{X}_\alpha) = \mathbf{x}_\alpha \quad \text{for all atoms } \alpha \in \Omega_0^{\mathrm{H}} \tag{7}$$

The compatibility conditions are imposed by Lagrange multipliers so the total energy functional is

$$\Pi = E_{\mathrm{total}} + \sum_{\alpha \in \Omega_0^{\mathrm{H}}} \int_{\Omega_0} \boldsymbol{\lambda}(\mathbf{X}) \cdot [\boldsymbol{\phi}(\mathbf{X}) - \mathbf{x}_\alpha] \delta(\mathbf{X} - \mathbf{X}_{\boldsymbol{\alpha}}) \, \mathrm{d}\Omega_0 \tag{8}$$

where $\boldsymbol{\lambda}$ is the vector of Lagrange multipliers that enforce the constraints and $\delta(\mathbf{X} - \mathbf{X}_{\boldsymbol{\alpha}})$ is Dirac delta function. We leave the above in an integral form because the Lagrange multipliers will be approximated by fields.

Equation (8) can be written by the following expression, which is generally adopted in the so-called 'handshake' method [2, 9],

$$E = E_{\mathrm{total}} + E_{\mathrm{MM/CM}} \tag{9}$$

where $E_{\mathrm{MM/CM}}$ is a coupling energy that corresponds to the second term in Equation (8). Note that by the well-known property of constrained minimization problems, the Lagrange multiplier term vanishes at the minimum, so the coupling energy vanishes provided the constraints are enforced exactly. In the method described here, the constraints are usually not satisfied exactly because as will be seen, we use an approximate Lagrange multiplier field rather than discrete multipliers. This gives rise to a residual interaction energy in the overlapping domain. The equilibrium configuration of the coupled model is obtained by determining the stationary point of the total energy functional Π in terms of $\boldsymbol{\phi}$, $\mathbf{x}_\alpha$, and $\boldsymbol{\lambda}$, as will be detailed in the next section.

2.2. Numerical implementation

The continuum domain is discretized by approximating the continuum deformation field and the Lagrange multiplier field by finite element interpolants with *nel* elements. Each element is mapped from the undeformed configuration to the current configuration through $\boldsymbol{\phi}^{\mathrm{e}}$. The deformed configuration for element e is expressed by

$$\boldsymbol{\phi}^{\mathrm{e}}(\mathbf{X}) = \sum_I N_I(\mathbf{X}) \boldsymbol{\phi}_I \tag{10}$$

DOI: 10.1002/nme

where $N_I(\mathbf{X})$ is the nodal shape function of node I, and $\boldsymbol{\phi}_I$ denotes the current nodal position. Similarly, the Lagrange multiplier field in the handshake domain is approximated by *mel* elements, with

$$\boldsymbol{\lambda}^{\mathrm{e}} = \sum_J N_J^{\lambda}(\mathbf{X})\boldsymbol{\lambda}_J \tag{11}$$

where $N_J^{\lambda}(\mathbf{X})$ is the shape function of the Lagrange multiplier field, and $\boldsymbol{\lambda}_J$ is the nodal value. Substituting the above equations to Equation (8) yields the discretized energy

$$\Pi = \sum_{\alpha\in\Omega_0^{\mathrm{A}}} \left[\sum_{\beta>\alpha} w^{\mathrm{A}} \left(\frac{1}{2}(\mathbf{X}_\alpha + \mathbf{X}_\beta) \right) V_{\alpha\beta} \right] + \int_{\Omega_0^{\mathrm{C}}} w^{\mathrm{C}}(\mathbf{X}) W(\mathbf{F}(\boldsymbol{\phi}))\, \mathrm{d}\Omega_0$$
$$- \int_{\partial\Omega_{\mathrm{t}}^{\mathrm{C}}} w^{\mathrm{C}}(\mathbf{X})\bar{\mathbf{t}} \cdot \mathbf{u}\, \mathrm{d}\Gamma_0 + \sum_{\alpha\in\Omega_0^{\mathrm{H}}} \sum_J N_J^{\lambda}(\mathbf{X}_\alpha)\boldsymbol{\lambda}_J \cdot \left[\sum_I N_I(\mathbf{X}_\alpha)\boldsymbol{\phi}_I - \mathbf{x}_\alpha \right] \tag{12}$$

Taking derivatives of the function with respect to $\mathbf{x}_\alpha$, $\boldsymbol{\lambda}_J$, and $\boldsymbol{\phi}_I$ yields the stationary condition for Π, which corresponds to the equilibrium equations and the constraint:

$$\frac{\partial \Pi}{\partial \boldsymbol{\phi}_I} = 0, \quad I = 1 \cdots n_{\mathrm{C}} \tag{13}$$

$$\frac{\partial \Pi}{\partial \boldsymbol{\lambda}_J} = 0, \quad J = 1 \cdots n_{\lambda} \tag{14}$$

$$\frac{\partial \Pi}{\partial \mathbf{x}_\alpha} = 0, \quad \alpha = 1 \cdots n_{\mathrm{A}} \tag{15}$$

where n_{C} is the number of finite element nodes, n_λ is the number of Lagrange multiplier nodes, and n_{A} is the number of the atoms in the coupled system. The resulting equations are

$$\mathbf{f}_I^{\mathrm{int}} + \sum_{J=1}^{n_\lambda} \mathbf{G}_{JI}\boldsymbol{\lambda}_J = \mathbf{f}_I^{\mathrm{ext}}, \quad I = 1 \cdots n_{\mathrm{C}} \tag{16}$$

$$\sum_{J=1}^{n_{\mathrm{C}}} \mathbf{G}_{IJ}\mathbf{u}_J = \mathbf{f}_I^{\lambda} \tag{17}$$

$$\sum_{\alpha\in\Omega_0^{\mathrm{A}}} \left[\sum_{\beta>\alpha} w^{\mathrm{A}} \left(\frac{1}{2}(\mathbf{X}_\alpha + \mathbf{X}_\beta) \right) \frac{\partial V_{\alpha\beta}}{\partial \mathbf{x}_\alpha} \right] - \sum_{\alpha\in\Omega_0^{\mathrm{H}}} \sum_J N_J^{\lambda}(\mathbf{X}_\alpha)\boldsymbol{\lambda}_J = 0 \tag{18}$$

where

$$\mathbf{f}_I^{\mathrm{int}} = \int_{\Omega_0^{\mathrm{C}}} w^{\mathrm{C}}(\mathbf{X}) \frac{\partial W}{\partial \mathbf{F}} \frac{\partial \mathbf{F}}{\partial \boldsymbol{\phi}_I}\, \mathrm{d}\Omega_0^{\mathrm{C}} \tag{19}$$

$$\mathbf{G}_{IJ} = \sum_{\alpha\in\Omega_0^{\mathrm{H}}} N_I^{\lambda}(\mathbf{X}_\alpha) N_J(\mathbf{X}_\alpha) \tag{20}$$

DOI: 10.1002/nme

$$\mathbf{f}_I^{\text{ext}} = \int_{\partial\Omega_t^C} w^C(\mathbf{X}) N_I(\mathbf{X}) \bar{\mathbf{t}} \, d\Gamma_0 \tag{21}$$

$$\mathbf{f}_I^{\lambda} = \sum_{\alpha \in \Omega_0^H} N_I^{\lambda}(\mathbf{X}_\alpha) \mathbf{u}_\alpha \tag{22}$$

where $\mathbf{u}_\alpha$ denotes the atomic displacement. The continuum forces can be expressed in terms of the first Piola–Kirchhoff stress $\mathbf{P}$ by noting that

$$\mathbf{P} = \frac{\partial W}{\partial \mathbf{F}} \tag{23}$$

and that

$$\frac{\partial \mathbf{F}}{\partial \boldsymbol{\phi}_I} = \frac{\partial N_I}{\partial \mathbf{X}} \tag{24}$$

which enables us to write Equation (19) as

$$\mathbf{f}_I^{\text{int}} = \int_{\Omega_0^C} w^C(\mathbf{X}) \mathbf{P} \frac{\partial N_I}{\partial \mathbf{X}} \, d\Omega_0^C \tag{25}$$

If the corresponding continuum model remains linear, the solution of Equations (16)–(18) can be simplified. We consider the case where $N_I^{\lambda}(\mathbf{X}) = N_I(\mathbf{X})$ in Ω^H. Let $\mathbf{d}_C$ be the continuum displacements in the subdomain exclusive of the handshake domain, $\mathbf{d}_H$ the continuum nodal displacements in the handshake domain, $\mathbf{d}_A$ the atomic displacements, i.e.

$$\mathbf{d}_C = \{\mathbf{u}_1, \ldots, \mathbf{u}_I, \ldots, \mathbf{u}_{n^C}\}^T, \quad I \in \Omega_0^C \setminus \Omega_0^H \tag{26}$$

$$\mathbf{d}_H = \{\mathbf{u}_1, \ldots, \mathbf{u}_I, \ldots, \mathbf{u}_{n^H}\}^T, \quad I \in \Omega_0^H \tag{27}$$

$$\boldsymbol{\lambda}^T = [\boldsymbol{\lambda}_1, \ldots, \boldsymbol{\lambda}_{n^H}] \tag{28}$$

$$\mathbf{d}_A = \{\mathbf{x}_1 - \mathbf{X}_1, \ldots, \mathbf{x}_\alpha - \mathbf{X}_\alpha, \ldots, \mathbf{x}_{n^A} - \mathbf{X}_{n^A}\}^T \tag{29}$$

For a linear continuum model, we can write

$$\mathbf{f}^{\text{int}} = \begin{Bmatrix} \mathbf{f}^C \\ \mathbf{f}^H \end{Bmatrix} = \begin{bmatrix} \mathbf{K}_C & \mathbf{K}_{CH} \\ \mathbf{K}_{CH}^T & \mathbf{K}_H \end{bmatrix} \begin{Bmatrix} \mathbf{d}_C \\ \mathbf{d}_H \end{Bmatrix} \tag{30}$$

where $\mathbf{K}_C$, $\mathbf{K}_{CH}$ and $\mathbf{K}_H$ are submatrices of the stiffness matrix $\mathbf{K}$ partitioned according to the partitioning of $\mathbf{d}$ (nodal displacement vector) into $\mathbf{d}_C$ and $\mathbf{d}_H$. Note that $\mathbf{f}^{\text{ext}}$ is partitioned into $\mathbf{f}_C^{\text{ext}}$ and $\mathbf{f}_H^{\text{ext}}$. We assume that there is no external force applied in handshake region. In a similar way $\mathbf{G}_C$ and $\mathbf{G}_H$ are obtained from $\mathbf{G}$, where $\mathbf{G}_C = 0$. Thus, the system of Equations (16)–(18) can be written as

$$\begin{bmatrix} \mathbf{K}_C & \mathbf{K}_{CH} & 0 & 0 \\ \mathbf{K}_{CH}^T & \mathbf{K}_H & 0 & \mathbf{G}_H^T \\ 0 & 0 & 0 & \mathbf{G}_A^T \\ 0 & \mathbf{G}_H & \mathbf{G}_A & 0 \end{bmatrix} \begin{Bmatrix} \mathbf{d}_C \\ \mathbf{d}_H \\ \mathbf{d}_A \\ \boldsymbol{\lambda} \end{Bmatrix} = \begin{Bmatrix} \mathbf{f}_C^{\text{ext}} \\ 0 \\ -\mathbf{f}_A^{\text{int}} \\ 0 \end{Bmatrix} \tag{31}$$

DOI: 10.1002/nme

where $\mathbf{G}_{\mathrm{A}J_\alpha} = -N_J^\lambda(\mathbf{X}_\alpha)$ and

$$\mathbf{f}_{\mathrm{A}}^{\mathrm{int}} = \sum_{\alpha\in\Omega_0^{\mathrm{A}}} \left[\sum_{\beta>\alpha} w^{\mathrm{A}} \left(\frac{1}{2}(\mathbf{X}_\alpha + \mathbf{X}_\beta) \right) \frac{\partial V_{\alpha\beta}}{\partial \mathbf{x}_\alpha} \right] \tag{32}$$

The nodal displacements $\mathbf{d}_{\mathrm{H}}$ can be found from the Schur complement of $\mathbf{K}_{\mathrm{H}}$, denoted by $\bar{\mathbf{K}}_{\mathrm{H}}$. The result is obtained by a simple rearrangement of the first two rows of the above

$$\mathbf{d}_{\mathrm{H}} = \bar{\mathbf{K}}_{\mathrm{H}}^{-1}(\mathbf{K}_{\mathrm{CH}}^{\mathrm{T}}\mathbf{K}_{\mathrm{C}}^{-1}\mathbf{f}_{\mathrm{C}}^{\mathrm{ext}} + \mathbf{G}_{\mathrm{H}}^{\mathrm{T}}\boldsymbol{\lambda}) \tag{33}$$

$$\bar{\mathbf{K}}_{\mathrm{H}} = \mathbf{K}_{\mathrm{CH}}^{\mathrm{T}}\mathbf{K}_{\mathrm{C}}^{-1}\mathbf{K}_{\mathrm{CH}} - \mathbf{K}_{\mathrm{H}} \tag{34}$$

Nodal displacements $\mathbf{d}_{\mathrm{C}}$ can be found in terms of $\mathbf{d}_{\mathrm{H}}$, using the first row of Equation (31) gives

$$\mathbf{d}_{\mathrm{C}} = \mathbf{K}_{\mathrm{C}}^{-1}(\mathbf{f}_{\mathrm{C}}^{\mathrm{ext}} - \mathbf{K}_{\mathrm{CH}}\mathbf{d}_{\mathrm{H}}) \tag{35}$$

Substituting Equation (33) into the last row of Equation (31) gives

$$\mathbf{A}\boldsymbol{\lambda} = \mathbf{f}^{\boldsymbol{\lambda}} \tag{36}$$

where

$$\mathbf{A} = \mathbf{G}_{\mathrm{H}}\bar{\mathbf{K}}_{\mathrm{H}}^{-1}\mathbf{G}_{\mathrm{H}}^{\mathrm{T}} \tag{37}$$

$$\mathbf{f}^{\lambda} = -(\mathbf{G}_{\mathrm{H}}\bar{\mathbf{K}}_{\mathrm{H}}^{-1}\mathbf{K}_{\mathrm{CH}}^{\mathrm{T}}\mathbf{K}_{\mathrm{C}}^{-1}\mathbf{f}_{\mathrm{C}}^{\mathrm{ext}} + \mathbf{G}_{\mathrm{A}}\mathbf{d}_{\mathrm{A}}) \tag{38}$$

For any given atomic configuration, $\{\mathbf{d}_{\mathrm{A}}\}$, $\mathbf{f}^{\lambda}$ can be calculated using Equation (38). The Lagrange multipliers $\boldsymbol{\lambda}$, and hence the continuum displacement field $\mathbf{u}$ can be determined by Equations (36) and (35), respectively.

For the coupled system under consideration, due to the constraints of the Lagrange multipliers, the system is not positive definite anymore and the solution is a saddle point. This makes many iterative methods inappropriate. Here, we use a quasi-Newton method BFGS [14] to determine the stationary point. Since the atomistic domain is free of any displacement constraint, a floating-domain problem is encountered when the calculated internal forces $\boldsymbol{\lambda}$ are not self-balanced i.e. in equilibrium, see Farhat and Roux [15] and Farhat *et al*. [16]. To overcome this difficulty, the following iteration procedure is used.

(1) Guess $\mathbf{d}_{\mathrm{A}}^n$, for $n = 1$.
(2) Solve Equation (36) for $\boldsymbol{\lambda}^n$.
(3) Update the finite element nodal positions using Equation (35).
(4) Search along the minimum direction of Π and update $\mathbf{d}_{\mathrm{A}}$ and Π.
(5) Check the convergence criterion $\|\Pi^{n+1} - \Pi^n\| < \varepsilon_\Pi$ and $\|\partial\Pi/\partial\mathbf{d}_{\mathrm{A}}\|_2 < \varepsilon_d$. If both are satisfied, an adequate equilibrium configuration has been obtained, otherwise, repeat from step (2).

We determine next the sufficient conditions for the regularity of $\mathbf{A}$ when $N_I^\lambda(\mathbf{X}) = N_I(\mathbf{X})$. Note that the rank of matrix product is given by

$$\mathrm{rank}(\mathbf{A}) \leqslant \mathrm{rank}(\mathbf{G}_{\mathrm{H}})\mathrm{rank}(\bar{\mathbf{K}}_{\mathrm{H}}) \tag{39}$$

DOI: 10.1002/nme

We assume that the stiffness matrix $\bar{\mathbf{K}}_{\mathrm{H}}$ is regular, since this is a standard property of finite elements. The matrix $\mathbf{G}_{\mathrm{H}}$ is assembled from element matrices $\mathbf{G}_{\mathrm{H}}^{\mathrm{e}}$ given by Equation (20), so

$$\mathbf{G}_{\mathrm{H}}^{\mathrm{e}} = \sum_{\alpha=1}^{n_{\alpha}^{\mathrm{e}}} \mathbf{N}^{\mathrm{T}}(\mathbf{X}_{\alpha})\mathbf{N}(\mathbf{X}_{\alpha}) \tag{40}$$

where n_{α}^{e} is the number of atoms in element e and $\mathbf{N} = [N_I]$. From the above, it follows that

$$(\mathbf{Z}_{\mathrm{e}})^{\mathrm{T}}\mathbf{G}_{\mathrm{H}}^{\mathrm{e}}\mathbf{Z}_{\mathrm{e}} \equiv \sum_{\alpha=1}^{n_{\alpha}^{\mathrm{e}}} \mathbf{Z}_I^{\mathrm{e}}\mathbf{N}_I(\mathbf{X}_{\alpha})\mathbf{N}_J(\mathbf{X}_{\alpha})\mathbf{Z}_J^{\mathrm{e}} = \sum_{\alpha=1}^{n_{\alpha}^{\mathrm{e}}} \mathbf{Z}^2(\mathbf{X}_{\alpha}) \tag{41}$$

The above can vanish for $\mathbf{Z}^{\mathrm{e}} \neq 0$ only if there exists a $\mathbf{Z}^{\mathrm{e}}$ such that

$$\sum_{I=1}^{n_{\mathrm{N}}^{\mathrm{e}}} N_I(\mathbf{X}_{\alpha})\mathbf{Z}_I^{\mathrm{e}} = 0, \quad \alpha = 1 \text{ to } n_{\alpha}^{\mathrm{e}} \tag{42}$$

where $n_{\mathrm{N}}^{\mathrm{e}}$ is the number of nodes in element e. If $n_{\alpha}^{\mathrm{e}} \geqslant n_{\mathrm{N}}^{\mathrm{e}}$, this can occur only if the locations of the points are degenerate, e.g. for a set of collinear points in a triangular element. Therefore, it follows that

$$(\mathbf{Z}_{\mathrm{e}})^{\mathrm{T}}\mathbf{G}_{\mathrm{H}}^{\mathrm{e}}\mathbf{Z}_{\mathrm{e}} > 0 \quad \forall \mathbf{Z}_{\mathrm{e}} \neq 0 \tag{43}$$

Therefore, all eigenvalues of $\mathbf{G}_{\mathrm{H}}^{\mathrm{e}}$ must be positive and by the element eigenvalue inequality [17], the eigenvalues of $\mathbf{G}_{\mathrm{H}}$ are positive. Thus, the rank must equal its dimension, and $\mathbf{A}$ must be regular.

Note that when the number of atoms in an element is less than the number of nodes or the positions of atoms are degenerate, the regularity of $\mathbf{A}$ is not ensured.

3. STRESS AND STRAIN IN THE COUPLED SYSTEM

In coupled continuum-molecular models based on overlapping decomposition methods, the stress and strain at the interface require careful definitions for consistency of the energy and smoothness. Here, we present a method for computing strain that provides a smooth strain field at the interface. We include both extensional and angle-bending terms. A method based on homogenization was recently presented by Chen and Fish [8].

The method is based on MLS approximation [18] of the displacement. In the MLS approximation, the displacement $\mathbf{u}(\mathbf{X})$ at any point $\mathbf{X}$ is approximated in the domain by

$$\mathbf{u}(\mathbf{X}) = \sum_{i=1}^{m} p_i(\mathbf{X})\mathbf{a}_i(\mathbf{X}) \tag{44}$$

where m is the number of terms in the basis $p_i(\mathbf{X})$ and $\mathbf{a}_i(\mathbf{X})$ are vector coefficients to be determined as described subsequently. The basis used here are polynomial so

$$[p_i(\mathbf{X})] = [1, X, Y] \quad \text{for a linear basis} \tag{45}$$

$$[p_i(\mathbf{X})] = [1, X, Y, X^2, XY, Y^2] \quad \text{for a quadratic basis} \tag{46}$$

$$\mathbf{a}_i = [a_{1i}, a_{2i}] = [a_{xi}, a_{yi}] \tag{47}$$

DOI: 10.1002/nme

The coefficients $\mathbf{a}$ at any point $\mathbf{X}$ are found by minimizing the weighted L_2 norm $q(\mathbf{X})$ given by

$$q(\mathbf{X}) = \sum_{\alpha \in S_{\mathbf{X}}} (p_i(\mathbf{X}_\alpha)\mathbf{a}_i(\mathbf{X}) - \mathbf{u}_\alpha)^{\mathrm{T}} w^{\mathrm{mls}}(\mathbf{X}_\alpha - \mathbf{X})(p_j(\mathbf{X}_\alpha)\mathbf{a}_j(\mathbf{X}) - \mathbf{u}_\alpha) \tag{48}$$

where a sum is implied over the repeated indices i and j, $w^{\mathrm{mls}}(\mathbf{X}_\alpha - \mathbf{X})$ is a weight function of compact support and $S_{\mathbf{X}}$ is the set of nodes within the support of $w^{\mathrm{mls}}(\mathbf{X}_\alpha - \mathbf{X})$. Various choices can be made for the weight functions (see [19]). We have chosen a cubic spline

$$w^{\mathrm{mls}}(r) = \begin{cases} \frac{2}{3} - 4r^2 + 4r^3 & \text{for } r \leqslant \frac{1}{2} \\ \frac{4}{3} - 4r + 4r^2 - \frac{4}{3}r^3 & \text{for } \frac{1}{2} < r \leqslant 1 \\ 0 & \text{for } r > 1 \end{cases} \tag{49}$$

where $r = \|\mathbf{X} - \mathbf{X}_\alpha\|/R_0$ and R_0 is the radius of the support circle centred at point $\mathbf{X}$. The radius of support depends on lattice constant; we have used $R_0 = 4l_0$, where l_0 is the equilibrium bond length (lattice constant).

The coefficients $\mathbf{a}_i(\mathbf{X})$ are found by minimizing $q(\mathbf{X})$ in Equation (48), which can be accomplished by finding the stationary point of $q(\mathbf{X})$. To develop these equations, we first adopt the more compact notation $p_{i\alpha} \equiv p_i(\mathbf{X}_\alpha)$, $w_\alpha \equiv w^{\mathrm{mls}}(\mathbf{X} - \mathbf{X}_\alpha)$, so Equation (48) becomes

$$q(\mathbf{X}) = \sum_{\alpha \in S_{\mathbf{X}}} (p_{i\alpha}\mathbf{a}_i - \mathbf{u}_\alpha)^{\mathrm{T}} w_\alpha(\mathbf{X}_\alpha - \mathbf{X})(p_{j\alpha}\mathbf{a}_j - \mathbf{u}_\alpha) \tag{50}$$

The stationary point of the above is then given by

$$0 = \frac{\partial q}{\partial \mathbf{a}_k} = \sum_{\alpha \in S_{\mathbf{X}}} p_{k\alpha} p_{j\alpha} w_\alpha \mathbf{a}_j - \sum_{\alpha \in S_{\mathbf{X}}} p_{k\alpha} w_\alpha \mathbf{u}_\alpha = 0 \tag{51}$$

which is a set of linear equations for $\mathbf{a}_j$. We note that the coefficient matrix of the left-hand side is the Gram matrix [20] M_{kj} (also called the moment matrix) given by

$$M_{kj} = \sum_{\alpha \in S_{\mathbf{X}}} p_{k\alpha} p_{j\alpha} w_\alpha \tag{52}$$

If we define

$$\mathbf{b}_k = \sum_{\alpha \in S_{\mathbf{X}}} p_{k\alpha} w_\alpha \mathbf{u}_\alpha \tag{53}$$

then Equation (51) can be written as

$$M_{kj}\mathbf{a}_j = \mathbf{b}_k \tag{54}$$

For a two-dimensional problem with a linear polynomial basis, the above is two systems of three equations in three unknowns.

The deformation gradient is then given by using its definition in conjunction with Equations (44) and (45). For a linear basis

$$\mathbf{F} = F_{ij} = \begin{bmatrix} 1 + a_{x2} & a_{x3} \\ a_{y2} & 1 + a_{y3} \end{bmatrix} \tag{55}$$

DOI: 10.1002/nme

The Green strain can be computed by the standard formula

$$\mathbf{E} = \tfrac{1}{2}(\mathbf{F}^{\mathrm{T}}\mathbf{F} - \mathbf{I}) \tag{56}$$

A noteworthy attribute of the MLS strain is that for a linear displacement of the atoms, the MLS strain gives the correct constant strain state. This may be seen as follows. Suppose that the displacements of the atoms are given by

$$\mathbf{u}_\alpha = \mathbf{u}(\mathbf{X}_\alpha) = p_i(\mathbf{X}_\alpha)\bar{\mathbf{a}}_i \tag{57}$$

Then substituting the above expression into the right-hand side of Equation (54) and using Equation (53) gives

$$M_{kj}\mathbf{a}_j = \mathbf{b}_k = \sum_{\alpha \in \mathrm{S}_\mathbf{X}} p_{k\alpha} w_\alpha p_{i\alpha} \bar{\mathbf{a}}_i \tag{58}$$

The right-hand side can be seen to be $M_{ki}\bar{\mathbf{a}}_i$ by Equation (52), so it follows that $\mathbf{a}_i = \bar{\mathbf{a}}_i$. It follows from Equations (55) and (56) that $\mathbf{E}$ also has the correct value. This is often called a reproducing condition: the MLS strain reproduces the strain associated with any displacements of the atoms derived from a linear field. Similarly, the MLS strain will reproduce the correct strain for any atomic displacements corresponding to a quadratic field.

In the handshake domain, the strains are obtained by weighing the atomistic strains and the continuum strains according to the weights in the energetics, Thus,

$$\mathbf{E}(\mathbf{X}) = w^{\mathrm{C}}(\mathbf{X})\mathbf{E}^{\mathrm{C}}(\mathbf{X}) + w^{\mathrm{A}}(\mathbf{X})\mathbf{E}^{\mathrm{A}}(\mathbf{X}) \tag{59}$$

The atomic stress is obtained in terms of doublets and triplets for the extensional and angle-bending potentials; the nomenclature is shown in Figure 1 (we depart temporarily from convention of Greek letters for atoms). The total potential W of the atomistic model is given by

$$W = \sum_{\substack{i,j \\ i>j}} W_{\mathrm{E}}^{ij} + \sum_{\substack{i,j,k \\ i>j>k}} W_{\mathrm{B}}^{ijk} \tag{60}$$

where W_{E}^{ij} is the extensional bond energy of the bond connecting atoms i and j and W_{B}^{ijk} is the bending energy of the triplet of atoms i, j and k.

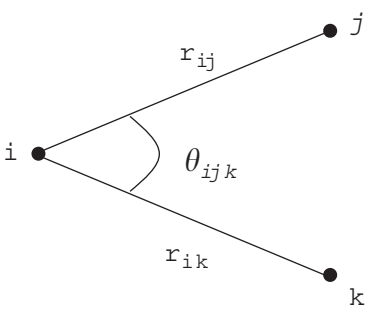

Figure 1. A triplet of atoms showing the bonds and bond angle.

DOI: 10.1002/nme

For a hexagonal lattice, a representative unit cell consists of three inequivalent bonds and two inequivalent nuclei. The strain-energy density of a representative unit cell with atom i as nucleus atom can be written as

$$\overline{W} = \frac{1}{2\Omega_0^n}\left[\sum_{j\in S^n} W_{\mathrm{E}}^{ij}(r^{ij}) + \frac{1}{2}\sum_{\substack{j,k\in S^n \\ j\neq k}} W_{\mathrm{B}}^{ijk}(\theta^{ijk})\right] \tag{61}$$

where S_n is a set of nearest neighbours of atom i in the unit cell. In the above r^{ij} is the length of bond between atoms i and j and θ^{ijk} is the angle subtended between bonds $\overline{ij}$ and $\overline{ik}$. In a hexagonal planar lattice, $\Omega_0^n = 3\sqrt{3}r_0^2 t/4$ is the volume occupied by each atom in the unit cell, where r_0 is the bond length (lattice constant) in the unstressed configuration and $t = 3.4\,\text{Å}$ is the nominal thickness of a graphene sheet. Note that the factor half on the right-hand side of the above equation appears due to the fact that the total energy is divided into two inequivalent nuclei. The other factor of half on the second term of right-hand side appears due to the double counting on the indices j and k.

To determine the atomic stresses, we use the relations between the continuum strain energy density W^{C}, after invoking the requirement that the continuum energy equals the discrete atomistic energy and the first Piola–Kirchhoff stress denoted by $\mathbf{P}$, and the Cauchy Born rule. The former gives that the first Piola–Kirchhoff stress is related to the potential by

$$\mathbf{P} = \frac{\partial W^{\mathrm{C}}}{\partial \mathbf{F}} = \overline{W}_{,\mathbf{F}} \tag{62}$$

The Cauchy stress $\boldsymbol{\sigma}$ will then be obtained by a standard transformation

$$\boldsymbol{\sigma} = \frac{1}{\det(\mathbf{F})}\mathbf{P}\mathbf{F}^{\mathrm{T}} \tag{63}$$

The Cauchy–Born rule [21] gives the following relation for any lattice vector $\mathbf{r}$ in terms of its value in the unstressed configuration $\mathbf{r}_0$:

$$\mathbf{r} = \mathbf{F}\mathbf{r}_0 \tag{64}$$

Using (61), (62) and (64), we now develop expressions for $\mathbf{P}$ in terms of the extensional and bending potentials. For this purpose, we use a simplified notation $\mathbf{a} = \mathbf{r}^{ij}$ and $\mathbf{b} = \mathbf{r}^{ik}$. The extensional potential gives

$$\mathbf{f}_{\mathrm{E}}^{ij} = W_{\mathrm{E}}^{ij}{}_{,\mathbf{a}} = W_{\mathrm{E}}^{ij}{}_{,a}\, a_{\mathbf{a}} = f^{ij}\frac{\mathbf{a}}{a} \tag{65}$$

where $f^{ij} = W_{\mathrm{E}}^{ij}{}_{,a}$; a is the length of the vector $\mathbf{a}$ and $\mathbf{a}/a$ is the unit vector that is collinear with that bond.

The angle-bending forces are given by

$$\mathbf{f}_{\mathrm{B}}^{ij} = W_{\mathrm{B}}^{ijk}{}_{,\mathbf{a}} = W_{\mathrm{B}}^{ijk}{}_{,C}\, C_{,\mathbf{a}} \tag{66}$$

$$\mathbf{f}_{\mathrm{B}}^{ik} = W_{\mathrm{B}}^{ijk}{}_{,\mathbf{b}} = W_{\mathrm{B}}^{ijk}{}_{,C}\, C_{,\mathbf{b}} \tag{67}$$

DOI: 10.1002/nme

where $C = \cos\theta$ and we have assumed the usual dependence of the angle-bending potential on the cosine of the angle θ between the bonds. From the formula for the scalar product $ab\cos\theta = \mathbf{a}\cdot\mathbf{b}$ it follows that

$$C_{,\mathbf{a}} = \frac{1}{ab}\left(\mathbf{b} - \frac{\mathbf{a}\cdot\mathbf{b}}{a^2}\mathbf{a}\right) \tag{68}$$

$$C_{,\mathbf{b}} = \frac{1}{ab}\left(\mathbf{a} - \frac{\mathbf{a}\cdot\mathbf{b}}{b^2}\mathbf{b}\right) \tag{69}$$

From (61), (62) and the chain rule we obtain

$$\mathbf{P} = \frac{1}{2\Omega_0^n}\left[\sum_{j\in S^n} W_{\mathrm{E}}^{ij}{}_{,\mathbf{a}}\,\mathbf{a}_{,\mathbf{F}} + \frac{1}{2}\sum_{\substack{j,k\in S^n \\ j\neq k}} (W_{\mathrm{B}}^{ijk}{}_{,\mathbf{a}}\,\mathbf{a}_{,\mathbf{F}} + W_{\mathrm{B}}^{ijk}{}_{,\mathbf{b}}\,\mathbf{b}_{,\mathbf{F}})\right] \tag{70}$$

From (64) it follows that

$$\mathbf{a}_{,\mathbf{F}} = \mathbf{I}\otimes\mathbf{a}_0, \quad \mathbf{b}_{,\mathbf{F}} = \mathbf{I}\otimes\mathbf{b}_0 \tag{71}$$

Using (65)–(67), we can rewrite (70) as

$$\mathbf{P} = \frac{1}{2\Omega_0^n}\left[\sum_{j\in S^n}\mathbf{f}_{\mathrm{E}}^{ij}\otimes\mathbf{a}_0 + \frac{1}{2}\sum_{\substack{j,k\in S^n \\ j\neq k}}\left(\frac{1}{ab}W_{\mathrm{B}}^{ijk}{}_{,C}\left(\mathbf{b} - \frac{\mathbf{a}\cdot\mathbf{b}}{b^2}\mathbf{a}\right)\otimes\mathbf{a}_0\right.\right.$$

$$\left.\left. + \frac{1}{ab}W_{\mathrm{B}}^{ijk}{}_{,C}\left(\mathbf{a} - \frac{\mathbf{a}\cdot\mathbf{b}}{a^2}\mathbf{b}\right)\otimes\mathbf{b}_0\right)\right] \tag{72}$$

Using Equations (63), (66)–(69), and the transformation $\Omega^n = \Omega_0^n \det(\mathbf{F})$, where Ω^n is the volume occupied by atom in the representative unit cell in current configuration and replacing $\mathbf{a}$ by $\mathbf{r}^{ij}$, $\mathbf{b}$ by $\mathbf{r}^{ik}$

$$\boldsymbol{\sigma} = \frac{1}{2\Omega^n}\left[\sum_{j\in S^n}\mathbf{f}_{\mathrm{E}}^{ij}\otimes\mathbf{r}^{ij} + \frac{1}{2}\sum_{\substack{j,k\in S^n \\ j\neq k}}(\mathbf{f}_{\mathrm{B}}^{ij}\otimes\mathbf{r}^{ij} + \mathbf{f}_{\mathrm{B}}^{ik}\otimes\mathbf{r}^{ik})\right] \tag{73}$$

The two terms in the second summation on the right-hand side of the above equation can be combined into one, as

$$\boldsymbol{\sigma} = \frac{1}{2\Omega^n}\left[\sum_{j\in S^n}\mathbf{f}_{\mathrm{E}}^{ij}\otimes\mathbf{r}^{ij} + \sum_{j\in S^n}\mathbf{f}_{\mathrm{B}}^{ij}\otimes\mathbf{r}^{ij}\right] \tag{74}$$

which is the standard virial stress form. As in the computation for the strain, a continuous stress field in the atomistic subdomain can be constructed using the MLS interpolation. The stress is computed by same weighting as the energetics in the handshake domain

$$\boldsymbol{\sigma}(\mathbf{X}) = w^{\mathrm{A}}(\mathbf{X})\boldsymbol{\sigma}^{\mathrm{A}}(\mathbf{X}) + w^{\mathrm{C}}(\mathbf{X})\boldsymbol{\sigma}^{\mathrm{C}}(\mathbf{X}) \tag{75}$$

DOI: 10.1002/nme

4. NUMERICAL EXAMPLES

In this section, several numerical examples are presented. Although the applicability of this method is not restricted to specific materials, we here choose graphene-like atomic sheets and carbon nanotubes (CNTs) as examples, because of their importance in engineering applications, as well as the simplicity of their atomic structures. To assess the performance of the coupled model, a full atomistic model corresponding to each example is solved independently, and compared with the coupled model.

4.1. Atomic sheet

Figure 2 shows a coupled model of an atomic sheet containing a double-vacancy defect in the centre. We use a quadratic interatomic potential that consists of a pair-body term and an angle-bending term:

$$E = E_{\text{stretch}} + E_{\text{angle}} \tag{76}$$

The pair-body term is piecewise quadratic, with

$$E_{\text{stretch}}(r) = \begin{cases} \frac{1}{2}k_{\text{a}}(r - r_0)^2 - \gamma, & r < r_{\text{c}} \\ \frac{1}{2}k_{\text{d}}(r - r_{\text{f}})^2, & r_{\text{c}} < r < r_{\text{f}} \\ 0, & r > r_{\text{f}} \end{cases} \tag{77}$$

where r_0 is the equilibrium distance, r_{c} and r_{f} are the bond lengths at which the interatomic force peaks and vanishes, respectively. The parameters k_{a} and k_{d} characterize the ascending and descending slopes of the force–separation curve, and γ is the potential energy when stretching the bond to infinite length. The parameters in the potential are chosen to ensure that the potential is piecewise continuous and differentiable. The interatomic force for this potential is then bilinear. The angle-bending term is of the following form:

$$E_{\text{angle}} = \tfrac{1}{2}k_\theta(\theta - \theta_0)^2[1 + k_{\text{sextile}}(\theta - \theta_0)^4] \tag{78}$$

Young's modulus and the Poisson's ratio can be then obtained through the Cauchy–Born rule [21]. Plane stress is assumed for the one-atom-thick sheet. The full atomistic model is set up such

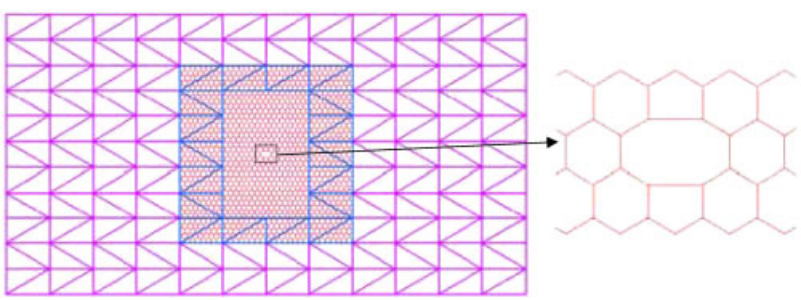

Figure 2. A coupled model of a graphene sheet containing a double-vacancy defect; a coarse model is shown for clarity.

DOI: 10.1002/nme

that each atom in the atomistic subdomain of the coupled model coincides with an atom in the full atomistic model. We will use two error criteria

(1) ε_{G}, the global error which measures the difference between the complete atomistic model and the coupled model in the entire domain Ω, and
(2) ε_{L}, the local error which measures the error in the atomistic subdomain Ω_0^{A} that is modelled by molecular mechanics.

Let $\mathbf{d}_{\mathrm{A}}$ be the atomic displacements as computed by the full atomistic model and $\mathbf{d}_{\mathrm{C}}$ the displacements at the atomic positions as computed by the coupled model. Then the global error is defined by

$$\varepsilon_{\mathrm{G}} = \frac{\|\mathbf{d}_{\mathrm{C}} - \mathbf{d}_{\mathrm{A}}\|_2}{\|\mathbf{d}_{\mathrm{A}}\|_2} \tag{79}$$

where

$$\|\mathbf{d}\|_2 = \left(\sum_i d_i^2\right)^{1/2} \tag{80}$$

The local error is computed by taking the restrictions of $\mathbf{d}_{\mathrm{A}}$ and $\mathbf{d}_{\mathrm{C}}$ to the subdomain Ω_0^{A}, which are denoted by $\mathbf{d}_{\mathrm{AL}}$ and $\mathbf{d}_{\mathrm{CL}}$, respectively, and given by

$$\varepsilon_{\mathrm{L}} = \frac{\|\mathbf{d}_{\mathrm{CL}} - \mathbf{d}_{\mathrm{AL}}\|_2}{\|\mathbf{d}_{\mathrm{AL}}\|_2} \tag{81}$$

To ensure that the edge atoms in the overlapping subdomain at the continuum–atomistic interface are properly co-ordinated, several additional rows of atoms are introduced. These additional atoms are often called virtual atoms or pad atoms [22]. Because of the angle-bending term in the potential, the pad thickness must be slightly larger than the cutoff radius of the atomistic covalent interaction. During the simulation, the positions of the pad atoms are determined by the continuum deformation field through interpolation by the finite element nodal displacements.

As a measure of the effectiveness of the coupling, we use the patch test, we apply a linear displacement field to the outside boundaries of a coupled model. In particular we let

$$u_{XI} = a_{x1} + a_{x2}X_I + a_{x3}Y_I \tag{82}$$

$$u_{YI} = a_{y1} + a_{y2}X_I + a_{y3}Y_I \tag{83}$$

where a_{xi} and a_{yi} are arbitrary constants. According to Equation (55), the deformation gradient should then be constant. The Green strain is computed by Equation (56). This test is applicable to arbitrary materials as long as the continuum material properties are consistent with the atomistic bond potential by the Cauchy–Born rule.

In our studies of the patch test, we avoided some of the difficulties in matching nonlinear atomistics with continua by using a harmonic potential and a Kirchhoff material with small prescribed displacements. We used $a_x = [0.5\ 0.02\ 0.02]$ and $a_y = [0.5\ 0.02\ 0.02]$. We used the error norm (79), with $\mathbf{d}_{\mathrm{A}}$ equal to the exact displacements by (82) and (83), to evaluate the performance of the method in the patch test.

The model is shown in Figure 3; the ratio of the lattice constant r_{L} to the largest dimension of the elements in the overlapping subdomain, h, $r_{\mathrm{L}}/h = 0.25$. The error $\varepsilon_{\mathrm{L}} = 0.2\%$, which is higher

DOI: 10.1002/nme

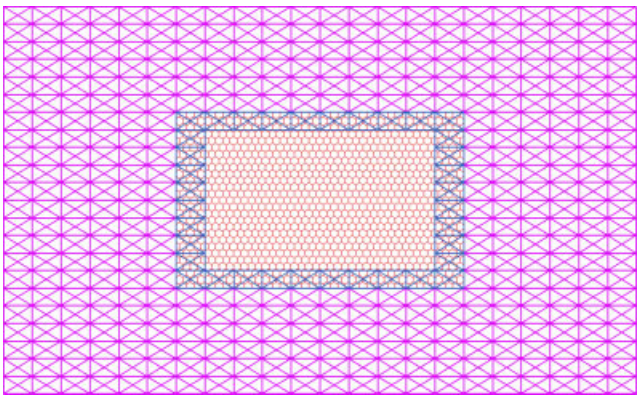

Figure 3. A coupled model of a graphene sheet used in patch test.

Table I. Results for the coupled model and the full atomistic model for the fracture of defected graphene sheets; σ_{frac} and $\varepsilon_{\text{frac}}$ are the fracture stress and strain, respectively, ε_{G} and ε_{L} are the global and local errors as given in Equations (79) and (81), respectively.

Model	# Atoms	# Nodes	ε_{G}	ε_{L}	σ_{frac} (GPa)	$\varepsilon_{\text{frac}}$
Coupled model I	360	528	0.026	0.189	59.5	17.8
Coupled model II	2174	477	0.030	0.062	56.8	16.7
Coupled model III	5544	366	0.028	0.033	57.8	16.7
Fully atomistic	10440	0	0.000	0.000	57.6	16.8

than expected. Most of the error comes from the handshake domain, where the strain differs as much as 1% from the prescribed value. In the atomistic domain, the maximum error in the strain is only 0.4%. This is adequate for most purposes, but indicates there is room for improvement in the method.

In the next example the size of the atomistic domain is varied while the size of the entire computational domain is fixed. Specifically, three sizes, small (39.3 Å × 22.7Å), medium (98.4 Å × 56.8 Å), and large (157.4 Å × 90.9 Å) atomistic domains are considered. The global and critical-subdomain errors are computed at around 75% of the fracture strain. For each model, the sheet is stretched in the y-direction by prescribing displacements to the nodes (or the atoms for the full atomistic model) on the edges ($y = \pm h$). At each prescribed displacement, the system is relaxed to its equilibrium configuration, and the corresponding applied tensile force is calculated. In the simulations, $k_{\text{a}} = 23.1\,\text{nN/Å}$, $k_{\text{d}} = -10.6\,\text{nN/Å}$, $\gamma = 2.22\,\text{eV}$, $r_0 = 1.42\,\text{Å}$, $r_{\text{c}} = 1.73\,\text{Å}$, and $r_{\text{f}} = 2.41\,\text{Å}$. The resulting Young's modulus and Poisson's ratio for the continuum are 326.8 GPa and 0.167, respectively.

Table I summarizes the results obtained by the coupled model and the full atomistic model. In calculating the stress, the nominal thickness of 3.4 Å for graphene is used. Our simulations show that with increasing size of atomistic domain, the local error progressively decreases, while the global error remains of the same order of magnitude. Except for the coupled model with the smallest atomistic domain, the other two coupled models yield fracture stresses and strains very

DOI: 10.1002/nme

close to those of the full atomistic model. Running time for five steps of 0.1% strain increment varied from 33.7 to 65.2 s from coupled model I to coupled model III, whereas fully atomistic model took 235.7 s.

We also studied the effects of finite element size on the accuracy of the computational results. An atomic sheet with dimensions of 393.52 Å $\times$ 227.20 Å is used for this study. The size of the atomistic subdomain is 196.76 Å $\times$ 113.06 Å. In the simulations, four different finite element sizes are chosen, namely, 4, 5, 10, and 20 lattice spacings. The corresponding local errors are 8.63×10^{-3}, 8.82×10^{-3}, 1.08×10^{-2}, 1.77×10^{-2}.

To illustrate the stress and strain computed by Equations (59) and (75), we consider an atomic sheet with a crack as an example. The dimensions of the sheet are 2262.75 Å $\times$ 1136.00 Å. The atomistic subdomain is 196.76 Å $\times$ 112.18 Å in size. An initial crack of 100 lattice spacings is introduced at the centre of the sheet with the crack surface perpendicular to the loading direction (y-direction). Due to the symmetry, only half of the sheet ($x \geqslant 0$) is modelled. The stress and the strain are calculated at the prescribed strain $\varepsilon_{yy} = 1\%$. Figure 4 shows the strain component ε_{yy}, and Figure 5 shows the equivalent stress (plane-stress is assumed for the continuum subdomain).

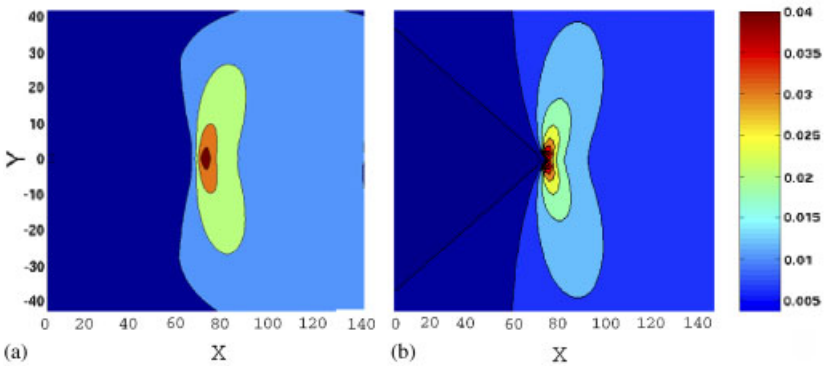

Figure 4. Contour of ε_{yy} around a crack tip for: (a) coupling model; and (b) linear elastic solution.

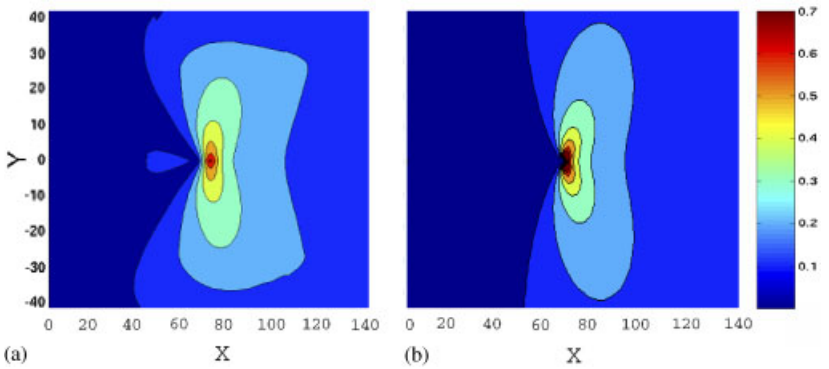

Figure 5. Contour of equivalent stress (in TPa) around a crack tip for: (a) coupling model; and (b) linear elastic solution.

DOI: 10.1002/nme

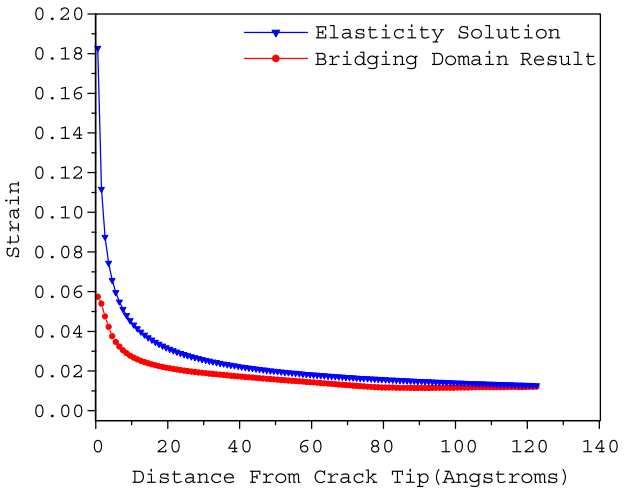

Figure 6. Strain along the crack calculated using coupling method and elasticity solution for a K-field.

Both the strain component and the equivalent stress agree well with those of the crack-tip fields based on continuum fracture mechanics. Strain calculated using coupling method for a K-field of strength 3 MPa$\sqrt{m}$ along the crack is also plotted in Figure 6 for a better comparison with the linear elastic closed-form solution and it can be seen that the error in the strain is quite small.

4.2. Fracture of CNTs

Next, we apply the coupled method to study the mechanical response of defected CNTs and multiwalled carbon nanotubes (MWCNTs) with different loading conditions (uniaxial tension and twisting). The modified second-generation Brenner potential [23] is used to describe interatomic interactions. Under applied load, the CNTs are deformed beyond the linear regime, so the continuum domain in the coupling method is characterized by a nonlinear constitutive law established through the exponential Cauchy–Born rule [24]. This nonlinear constitutive law has been used to study the collapse of CNTs [25, 26].

Figure 7 shows the coupled model of a single-walled [50, 0] CNT containing a double vacancy defect in the centre. Fracture of small nanotubes containing such a defect has also been studied quantum mechanically [27]. The atomistic domain contains 1898 atoms, while the continuum domain consists of 1040 finite element nodes. The tube is 142 Å in length, the atomistic domain is 39.15 Å long and the overlapping subdomain is 11.36 Å long. Thus, the overlapping boundary is far enough away from the defect so that the displacement field can be accurately characterized by the finite element model. The full atomistic model of the tube consists of 6698 atoms.

For the continuum domain in the coupled nanotube model, the subdivision finite elements based on Loop's scheme [28] are used. The deformation field within each triangular element depends not only on the nodal coefficients of its three nodes, but also on those of its first neighbouring nodes. Subdivision element difficulties arise for the triangular elements at the continuum/atomistic interfaces, for they lack neighbouring elements. Thus, in the coupled model, besides adding pad atoms,

DOI: 10.1002/nme

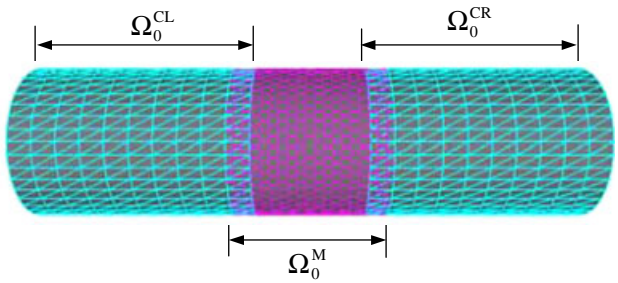

Figure 7. Coupled model for a [50, 0] CNT; ($\Omega_0^C = \Omega_0^{CL} \cup \Omega_0^{CR}$ and $\Omega_0^H = \Omega_0^C \cap \Omega_0^M$).

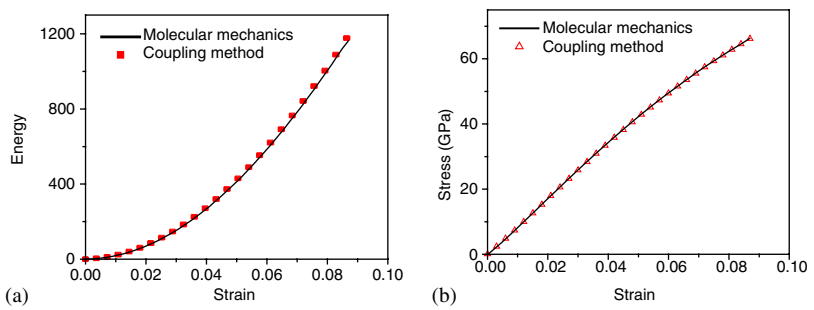

Figure 8. Energetics (a) and stress–strain curves (b) of stretched [50, 0] CNT.

virtual finite element nodes are needed to ensure that the edge nodes at the continuum/atomistic interfaces are appropriately co-ordinated. Thus, an extra row of elements extends into the continuum domain. The finite element nodal positions of these virtual elements are determined by minimizing the difference between the atomistic displacement and the interpolated continuum displacement:

$$\eta = \sum_{\alpha} \left\| \sum_{I} N_I(\mathbf{X}_\alpha)\boldsymbol{\phi}_I - \mathbf{x}_\alpha \right\|^2 \tag{84}$$

for all nodes I in the pad elements. Note that the energy associated with the pad atoms and pad elements is not accounted for in the total free energy of the coupled system.

Figure 8 shows the results for the nanotube stretched to fracture. Figure 8(a) shows the energy evolution of the tube as a function of applied tensile strain. At small strains, the internal energies provided by these two models are almost indistinguishable. As the applied strain increases, the total energy predicted by the coupled model deviates slightly from the atomistic model. Figure 8(b) shows stress–strain curves obtained by these two methods, which are almost indistinguishable.

Figure 9 shows the energy evolution of the CNT twisted up to 20° by rotating its ends in opposite directions with respect to the axis of the tube. As in uniaxial tension, the energetics predicted by the two models is almost identical at small rotation angles, and deviates only slightly from each other at large strains. Figure 10 compares the configurations predicted by these two models

DOI: 10.1002/nme

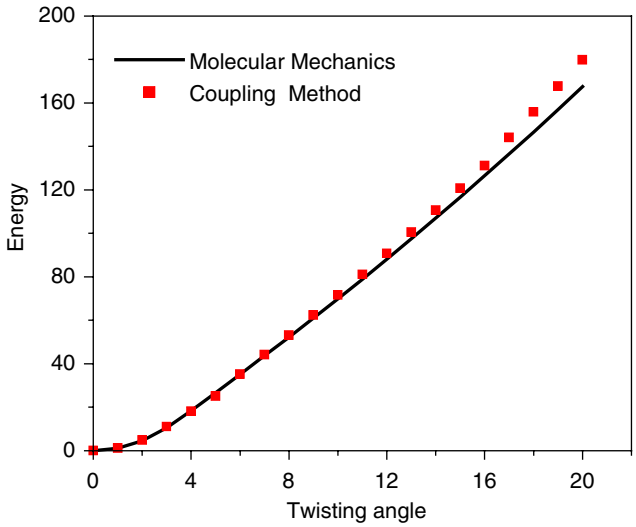

Figure 9. Energetics of twisted [50, 0] CNT.

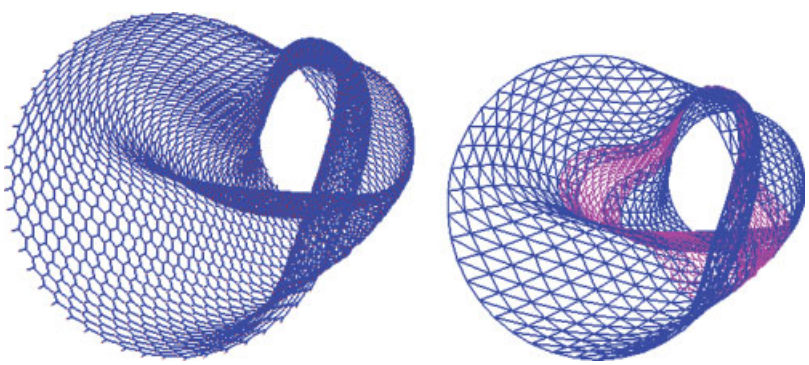

Figure 10. Configuration of twisted [50, 0] CNT.

at 15° rotation. It can be seen that the coupled calculation captures all of the features of the full atomistic model.

The next example serves to illustrate how the atomistic model can easily be moved around once a model has been constructed. Figure 11 shows a three walled CNT in which the atomistic model has been replaced in two locations, first in the centre of the tube, next near the support. In each case, the finite element model is modified by setting the material properties of the domain to be overlaid to zero. Note that the mesh of the finite element model is unchanged. Thus, once the finite element model has been constructed, defects in various locations of the model can easily be studied. Details of how the van der Waals forces between adjacent continuum and continuum/atomistic models are treated are given in [29].

DOI: 10.1002/nme

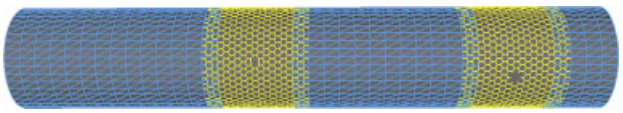

Figure 11. A MWCNT with two defects.

5. CONCLUDING REMARKS

A coupling method for bridging molecular mechanics and finite element methods has been presented. The method is based on an overlapping domain-decomposition scheme. Displacement compatibility conditions in the overlapping subdomain are enforced by Lagrange multipliers. A faster formulation has been developed for the case where the continuum domain is linear elastic. An important advantage of the method is that it does not require the finite element nodes to match the atoms at the interface. Such matching is a requirement in many handshake methods, i.e. [2, 3], and is quite awkward. In this method, a crystal lattice with an arbitrary lattice constant can be linked to any finite element mesh, although of course, the disparity between the mesh and lattice size should not be too large. This facilitates the placement of the atomistic model in any part of the body: to replace the continuum model anywhere by an atomistic model, it is only necessary to zero the material constants in a subdomain and superimpose the atomistic model.

A method has also been presented for computing strains based on a MLS fit. The method exactly reproduces a strain state one order lower than the polynomial basis. Thus, for a linear basis, the method gives the exact strain for atoms in a linear displacement field. In contrast to the Mott *et al*. [13] atomistic strain, this method does not require a Voronoi tessellation, so it is much easier to implement.

A patch test has been described for the coupling method. The performance of this proposed coupling method in the patch test was adequate, but some irregularities were noted in the strain in the overlapping domain. We are further investigating the source of these discrepancies.

Numerical examples studying the mechanical responses of defected atomic sheets and CNTs are presented. Comparisons between the coupled models and the corresponding fully atomistic models show very good agreement. This suggests that for most applications, the method is quite satisfactory.

ACKNOWLEDGEMENTS

We gratefully acknowledge the grant support from the NASA University Research, Engineering and Technology Institute on Bio Inspired Materials (BIMat) under award No. NCC-1-02037 and the support of the Army Research Office under grant.

REFERENCES

1. Rudd RE, Broughton JQ. Concurrent coupling of length scales in solid state systems. *Physica Status Solidi B* 2000; **217**:251–291.
2. Abraham FF, Broughton JQ, Bernstein N, Kaxiras E. Spanning the length scales in dynamic simulation. *Computational Physics* 1998; **12**(6):538–546.
3. Wagner GJ, Liu WK. Coupling of atomistic and continuum simulations using a bridging scale decomposition. *Journal of Computational Physics* 2003; **190**(1):249–274.

DOI: 10.1002/nme

4. Park HS, Karpov EG, Liu WK. Non-reflecting boundary conditions for atomistic, continuum and coupled atomistic/continuum simulations. *International Journal for Numerical Methods in Engineering* 2005; **64**(2): 237–259.
5. Belytschko T, Xiao SP. Coupling methods for continuum model with molecular model. *International Journal for Multiscale Computational Engineering* 2003; **1**(1):115–126.
6. Xiao SP, Belytschko T. A bridging domain method for coupling continua with molecular dynamics. *Computer Methods in Applied Mechanics and Engineering* 2004; **193**:1645–1669.
7. Shilkrot LE, Miller RE, Curtin WA. Multiscale plasticity modeling: coupled atomistics and discrete dislocation mechanics. *Journal of the Mechanics and Physics of Solids* 2004; **52**(4):755–787.
8. Chen W, Fish J. A generalized space-time mathematical homogenization theory for bridging atomistic and continuum scales. *International Journal for Numerical Methods in Engineering* 2006; **67**(2):253–271.
9. Curtin WA, Miller RE. Atomistic/continuum coupling in computational materials science. *Modelling and Simulation in Materials Science and Engineering* 2003; **11**(3):R33–R68.
10. Ghoniem NM, Busso EP, Kioussis N, Huang H. Multiscale modelling of nanomechanics and micromechanics: an overview. *Philosophical Magazine* 2003; **83**:3475–3528.
11. Liu WK, Karpov EG, Zhang S, Park HS. An introduction to computational nanomechanics and materials. *Computer Methods in Applied Mechanics and Engineering* 2004; **193**(17–20):1529–1732.
12. Dhia HB, Rateau G. The Arlequin method as a flexible engineering desing tool. *International Journal for Numerical Methods in Engineering* 2005; **62**:1442–1462.
13. Mott PH, Argon AS, Suter UW. The atomic strain tensor. *Journal of Computational Physics* 1992; **101**:140–150.
14. Liu DC, Nocedal J. On the limited memory method for large scale optimization. *Mathematical Programming B* 1989; **45**(3):503–528.
15. Farhat C, Roux FX. A method of finite element tearing and interconnecting and its parallel solution algorithm. *International Journal for Numerical Methods in Engineering* 1991; **32**:1205–1227.
16. Farhat C, Li J, Avery P. A FETI-DP method for parallel iterative solution of indefinite and complex-valued solid and shell vibration problems. *International Journal for Numerical Methods in Engineering* 2005; **63**(3):398–427.
17. Belystchko T, Liu WK, Moran B. *Nonlinear Finite Elements for Continua and Structures*. Wiley: New York, 2001.
18. Belytschko T, Lu YY, Gu L. Element-free Galerkin methods. *International Journal for Numerical Methods in Engineering* 1994; **37**:229–256.
19. Belytschko T, Krongauz Y, Organ D, Fleming M, Krysl P. Meshless methods: an overview and recent developments. *Computer Methods in Applied Mechanics and Engineering* 1996; **139**(1–4):3–47.
20. Huerta A, Mendez SF. Enrichment and coupling of the finite element and meshless methods. *International Journal for Numerical Methods in Engineering* 2000; **48**:1615–1636.
21. Arroyo M, Belytschko T. Finite element methods for the non-linear mechanics of crystalline sheets and nanotubes. *International Journal for Numerical Methods in Engineering* 2004; **59**:419–456.
22. Shilkrot LE, Curtin WA, Miller RE. A coupled atomistic/continuum model of defects in solids. *Journal of the Mechanics and Physics of Solids* 2002; **50**(10):2085–2106.
23. Shenderova OA, Brenner DW, Omeltchenko A, Su X, Yang LH. Atomistic modeling of the fracture of polycrystalline diamond. *Physical Review B* 2000; **61**(6):3877–3888.
24. Arroyo M, Belytschko T. Finite crystal elasticity of carbon nanotubes based on the exponential Cauchy–Born rule. *Physical Review B* 2004; **69**(14):115415.
25. Zhang S, Khare R, Belytschko T, Hsia KJ, Mielke SL, Schatz GC. Transition states and minimum energy pathways for the collapse of carbon nanotubes. *Physical Review B* 2006; **73**(7):075423.
26. Arroyo M, Belytschko T. A finite deformation membrane based on inter-atomic potentials for the transverse mechanics of nanotubes. *Mechanics of Materials* 2003; **35**(3–6):193–215.
27. Mielke SL, Troya D, Zhang S, Li J-L, Xiao S, Car R, Ruoff RS, Schatz GC, Belytschko T. The role of vacancy defects and holes in the fracture of carbon nanotubes. *Chemical Physics Letters* 2004; **390**(4–6):413–420.
28. Cirak F, Ortiz M, Schroeder P. Subdivision surfaces: a new paradigm for thin-shell finite-element analysis. *Computer Methods in Applied Mechanics and Engineering* 1999; **193**:1645–1669.
29. Zhang S, Mielke SL, Khare R, Troya D, Ruoff RS, Schatz GC, Belytschko T. Mechanics of defects in carbon nanotubes: atomistic and multiscale simulations. *Physical Review B* 2005; **71**(115403).

DOI: 10.1002/nme